Dissociative recombination and excitation of N_2^+: Cross sections and product branching ratios

Cite as: J. Chem. Phys. **108**, 1978 (1998); https://doi.org/10.1063/1.475577
Submitted: 11 August 1997 . Accepted: 27 October 1997 . Published Online: 04 June 1998

J. R. Peterson, A. Le Padellec, H. Danared, G. H. Dunn, M. Larsson, A. Larson, R. Peverall, C. Strömholm, S. Rosén, M. af Ugglas, and W. J. van der Zande

Dissociative recombination and excitation of N_2^+: Cross sections and product branching ratios

J. R. Peterson
Molecular Physics Laboratory, SRI International, Menlo Park, California 94025

A. Le Padellec
Department of Physics, Royal Institute of Technology (KTH), S-100 44 Stockholm, Sweden

H. Danared
Manne Siegbahn Laboratory, Stockholm University, S-104 05 Stockholm, Sweden

G. H. Dunn
Manne Siegbahn Laboratory, Stockholm University, S-104 05 Stockholm, Sweden and JILA, University of Colorado and NIST, Boulder, Colorado 80309-0440

M. Larsson
Department of Physics, Stockholm University, Box 6730, S-113 85, Stockholm, Sweden

A. Larson
Department of Physics, Royal Institute of Technology (KTH), S-100 44 Stockholm, Sweden

R. Peverall
FOM-Institute for Atomic and Molecular Physics, Kruislaan 407, 1098 SJ Amsterdam, The Netherlands

C. Strömholm and S. Rosén
Department of Physics, Royal Institute of Technology (KTH), S-100 44 Stockholm, Sweden

M. af Ugglas
Manne Siegbahn Laboratory, Stockholm University, S-104 05 Stockholm, Sweden

W. J. van der Zande
FOM-Institute for Atomic and Molecular Physics, Kruislaan 407, 1098 SJ Amsterdam, The Netherlands

(Received 11 August 1997; accepted 27 October 1997)

The absolute dissociative recombination and absolute dissociative excitation rate coefficients and cross sections have been determined for N_2^+ and electrons for collision energies between 10 meV and 30 eV. The ion storage ring CRYRING has been used in combination with an imaging technique with a position-and-time-sensitive detector. Information is retrieved on the ion beam vibrational state populations and on the product branching in the dissociative recombination process at 0 eV collisions. A hollow cathode ion source has been used to lower the vibrational excitation in the ion beam; a more traditional hot-cathode ion source was used as well. The most important findings are the following. The rate coefficient for an N_2^+ ion beam (46%, $v=0$, 27% $v=1$) *versus* electron temperature (K) is $\alpha(T_e)=1.75(\pm 0.09)\times 10^{-7}(T_e/300)^{-0.30}$ cm^3 s^{-1}. The dissociative recombination rate is found to be weakly dependent on the N_2^+ vibrational level. At 0 eV collision energy, the $v=0$ product branching is found to be 0.37(8):0.11(6):0.52(4) for $N(^4S)+N(^2D)$:$N(^2P)+N(^4S)$:$N(^2D)+N(^2D)$ fragments. The dissociative recombination cross section does not have a high-energy peak as was found in a number of lighter molecular systems. The dissociative excitation signal starts only slightly above the energy threshold for dissociation, and peaks near 25 eV. From the dissociative excitation data and literature data, information is retrieved on the dissociative ionization of N_2^+. The comparison of these results with earlier DR measurements is extensively discussed. [S0021-9606(98)02405-2]

I. INTRODUCTION

Dissociative recombination (DR) is a process of considerable importance for the chemistry of natural as well as manmade plasmas. Over the last few years the storage ring technique has been applied to the study of this process, and the new experimental possibilities have improved substantially our ability to study the dissociative recombination process.[1,2] Over the last few years, absolute cross sections have been reported for various molecular systems. Product branching information has been determined for the diatomics H_2^+ and HD^+,[3,4] HeH^+, and HeD^+,[5,6] and CH^+,[7] and polyatomic ions such as H_3^+,[8] H_2D^+,[9] H_2O^+, H_3O^+, and CH_3^+,[10] and CH_5^+.[11] The possibility to store molecular ions in an ion storage ring often simplifies interpretation of the results, because internal modes of the molecular ions may relax radiatively towards the ground-state energy within the storage time.

This paper presents the first storage ring DR absolute rate coefficient and cross-section measurements for electronic ground-state $^{14}N_2^+$ ions. Due to the lack of a dipole moment, the homonuclear N_2^+ ions do not cool by radiative

processes. In order to have as vibrationally cold nitrogen ions as possible, we used a high-pressure hollow cathode discharge source. The vibrational population could be monitored indirectly by using a three-dimensional imaging technique to determine N-atom product state distributions. Using the ion storage ring ASTRID, Kella *et al.*[12] have reported product branching earlier using a two-dimensional imaging technique. In this paper we present cross-section data over a wide energy span ranging from 10 meV to 30 eV not only for dissociative recombination but also for dissociative excitation. We also report accurate product state information at 0 eV collisions using ion beams with different vibrational populations.

The N_2^+ ion belongs to the family of the earth's atmospheric ions, of which other members are NO^+ and O_2^+, and it is closely involved in the chemistry of planetary ionospheres.[13,14] Under atmospheric conditions, provided that the concentrations of neutral species are high enough, ion–molecule reactions are the dominating sink for molecular ions with high ionization potentials, such as N_2^+ and O_2^+. If the neutral densities decrease, dissociative recombination dominates as the sink for low-energy electrons and molecular ions. This is the situation at higher altitudes. Dissociative recombination exhibits a high exothermicity, which makes DR the only source of kinetically energetic atoms (>1 eV). The exothermicity is shared among the various internal states and the kinetic energies of the atomic fragments (N or O); this gives rise to a myriad of atmospheric phenomena, such as airglows. Thus, the study of DR mechanisms for these atmospheric ions is of special interest, not only the determination of the absolute efficiencies but also the branching into the different accessible exothermic channels.

One interesting phenomenon ascribed to DR-processes in N_2^+, is the possible isotopic fractionation resulting from the selective escape of ^{14}N atomic nitrogen from the atmosphere of Mars.[15,16] Among all the exothermic dissociative channels, one channel is sufficiently exothermic to account for an isotope-selective escape:

$$N_2^+(v=0)+e^-\rightarrow N(^4S)+N(^2D)+3.45\ \text{eV}.$$

The escape is only possible above the so-called exobase, which delimits the collision zone from the collisionless zone in the atmosphere. At lower altitudes, collisions slow down the N fragments, obstructing escape. A preferential escape of the ^{14}N over ^{15}N may explain the unusual isotopic $^{15}N/^{14}N$ ratio found in the Martian atmosphere.[17]

Due to its central role in the chemistry of planetary atmospheres including our own atmosphere, the N_2^+ ion has been the subject of research over the last five decades. Pioneering work by Biondi and Brown[18] led to reliable results by Kasner[19] as early as 1967, who reported a rate coefficient of 2.7×10^{-7} cm^3 s^{-1} at room temperature with a stationary afterglow setup. This was followed up using the same kind of device by Mehr and Biondi,[20] who found 1.8×10^{-7} cm^3 s^{-1} at the same temperature. Later, in 1971, Mahdavi *et al.*,[21] using a flowing-afterglow Langmuir-probe apparatus (FALP), recorded a rate coefficient of 2.2×10^{-7} cm^3 s^{-1} at 300 K, but their analysis procedure did not take into account the presence of possible recombining impurities in the afterglow. Cunningham and Hobson[22] applied the shock tube technique to N_2^+ and found a rate coefficient of 1.8×10^{-7} cm^3 s^{-1} at room temperature; they gave this result as the DR rate coefficient for vibrational ground-state ions. Although in their technique the vibrational temperature of the ions could be varied, and DR rates were obtained for higher temperatures, it is possible that the gas temperature and the ionic composition could differ behind the front of the shock wave, which complicated these experiments in a serious manner. Zipf[23] coupled a microwave afterglow with a laser-induced-fluorescence setup to measure DR rate coefficients as a function of vibrational quantum number up to $v=3$. For $v=0$, the rate coefficient was measured to be 2.2×10^{-7} cm^3 s^{-1}, in excellent agreement with the other values stated above. Nevertheless, Zipf's experiment has been challenged by Johnsen,[24] who suggested that instead of measuring vibrational-state-resolved rates the experiment of Zipf produced an effective rate coefficient corresponding to a vibrational temperature of about 1500 K. Noren *et al.* using a single-pass merged beams apparatus reported controversial results.[25] The rate coefficients inferred from the absolute cross-section measurements are a factor of 5 smaller than those obtained by the experiments reviewed above. This large discrepancy has been one of the motivations for the present experiments. More recently, Geoghegan *et al.*[26] reported a value of 2×10^{-7} cm^3 s^{-1} and Canosa *et al.*[27] a rate coefficient of 2.6×10^{-7} cm^3 s^{-1} for vibrational ground-state N_2^+ at room temperature, both using the flowing-afterglow Langmuir-probe mass spectrometer technique. In conclusion, the various measurements agree within about 50% of each other with the exception of the single-pass merged-beams experiment. The present data are in approximate quantitative agreement with the majority of the results for 300 K. The present experiment adds results at electron collisions energy range between 0.003 and 30 eV. In addition, the atomic fragment final state distributions are determined from the data for the first vibrational levels, $v=0-3$.

II. EXPERIMENT

The experimental setup has been described previously in considerable detail.[2,5,28] We limit ourselves here to a brief description, and concentrate instead on developments necessary for the present measurements. Figure 1 shows the layout of the CRYRING apparatus. The N_2^+ ions are extracted from an ion source (see below), accelerated to 40 keV, mass analyzed, focused, and injected into the ring. The ring has a circumference of 51 m. The ring parameters limit the energy of the ions to $96q^2/M$ (MeV), with q the charge and M the ion mass, in atomic mass units. This yields for N_2^+ a maximum beam energy of 3.4 MeV. After acceleration, the ions coast in the ring. In each revolution the ions encounter a straight section containing a uniform electron beam of about 85 cm length, 4 cm diam, and current of about 1.25 mA. This beam is referred to as the ''cooler,'' since in normal opera-

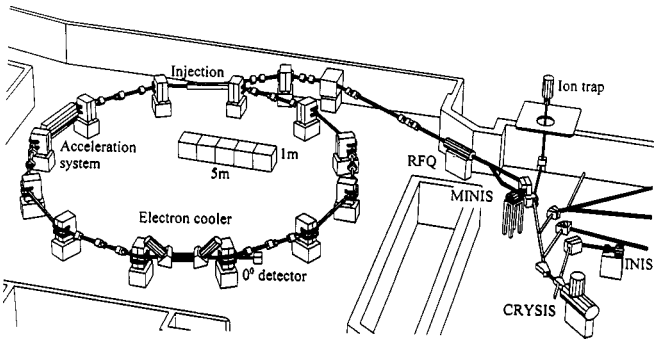

FIG. 1. Layout of the storage ring facility CRYRING. An N_2^+ ion beam from two different ion sources (MINIS and JIMIS, see text) are injected in the ring at 40 keV and further accelerated to 3.4 MeV. In the cooler section the ions interact with electrons, the neutral products enter the 0°-arm and are detected on a surface barrier detector (SBD, 3 meter behind the cooler) or a three-dimensional imaging detector (3D-ID) 6.3 m behind the cooler.

tion of the ring the electrons in this beam phase space cool the ions. This normally has the effect of reducing the diameter of the ion beam and ensuring that the ions and electrons are longitudinally aligned. However, the present ions have such a low charge to mass ratio, (q/M), that the effectiveness of the electrons in cooling the ions is negligible in the time frame of the experiments. Extra efforts involving maximizing the recombination rate with the voltage and alignment of the cooler were therefore necessary in order to locate the zero of energy, and to ensure the alignment of the electron and ion beams (necessary for optimum energy resolution in the studies). Therefore, in this experiment, the cooler provides nothing more than a dense cold target of electrons of varying energy with which the ions collide.

The collisions of interest here are those resulting in DR and dissociative excitation (DE). For DR, the resulting (two) neutral fragments leave the ring at the first dipole magnet and enter the so-called zero-degree arm which is equipped with a surface barrier detector (SBD), and an imaging detector (ID) which is positioned 6.3 m behind the electron cooler. The SBD, which can be moved in our out of the zero-degree arm, is used to determine the absolute DR-rates. From the SBD, DR-signal (two N-atoms) is readily distinguished from background and DE events (one N-atoms). Using a multichannel analyzer (MCA), the number of background counts is recorded simultaneously with DR counts. The N-atom background is due predominantly to dissociation of N_2^+ ions by: (a) Collisions with background gas (B_g); and (b) collisions with slow ions which have been formed by electron bombardment of the background gas, and trapped in the space charge of the electron beam (B_i). Since both B_g and B_t are proportional to background pressure, and as the pressure in the system is constant during the run, the number of counts in the background is used as a measure of the *number of circulating ions*. In an independent experiment an absolute current measurement in the ring is tied to a background SBD measurement. For these measurements, the absolute count rates in the N and 2N channels of the SBD are monitored with a multichannel scaler (MCS). After determination of the electron current and using the fact that the electron beam is homogenous with a diameter of 4 cm and an interaction length of 85 cm, the ratio of signal (N_2) to background (N) counts is transformed to an *absolute rate*. For a more extensive description of the procedure see Strömholm *et al.*[5]

The MCA measurements are repeated at each interaction energy for which data are desired. If E_{cool} is the laboratory energy where the average relative energy between ions and electrons is zero and E_{meas} is the laboratory energy at which a new measurement is wanted, then the relation between the new center of mass energy, E_d, and these laboratory energies is given in principle by the simple algorithm, $(E_d)^{1/2} = (E_{\mathrm{meas}})^{1/2} - (E_{\mathrm{cool}})^{1/2}$. A small correction is necessary to account for the electron space charge correction which is partially neutralized by ions trapped in the electron beam and which is not the same at different values of E_{meas}. The space charge correction can easily be calibrated at 0 eV, the cooling energy. However, especially at the low electron beam energies (66 eV) when working with ''heavy'' molecular ions as N_2^+ at 3.4 MeV, the quantification of the space charge correction at elevated electron collision energies results in a 30 meV uncertainty in the absolute collision energy at around 1 eV collision energy.[29,30]

Detecting N atoms in the MCS mode is also used at various energies to study dissociative excitation $(N_2^+ + e^- \rightarrow N + N^+ + e^-)$. The protocol here is to alternate the potential of the cooler between E_{cool} and E_{meas} and collect data for a few seconds at each energy, continuing the switching for as long as the ions last. A new set of ions is then loaded and the measurements are repeated giving correlated data into the same scaler bins until enough counts are in each bin to result in good precision. DE results in a jump in the count rate in the N-atom channel upon the cooler jump. The DE signal is also used in the DR-rate measurements in the form of a correction of the number of N-atom counts, which is used as a measure of the ion beam current in the ring.

At an ion beam energy of 3.4 MeV, collisions with residual gas still result in an appreciable charge transfer signal. This is counted in the N_2 channel and contributes to the signal. The charge transfer contribution was measured by monitoring the observed rate of (N_2)-signal using the MCS while switching the electron cooler current on and off.

Unfolding the energy dependent cross section from the observed absolute rates requires simply a division by the average velocity at ''higher'' collision energies (> 50 meV) and a correction for the change in electron density upon changing the electron beam energy. At smaller energies a deconvolution procedure has been described in detail[31] that allows for the extraction of absolute cross-section data down to a few meV collision energy.

A. Ion sources

In order to measure cross sections and rates that are valid for applications such as sparsely ionized planetary ionospheres, where the density and ionization are such that the recombination occurs slowly enough that all ions are in the ground vibrational state, it is desirable to measure the rates for vibrational ground-state ions. In most cases, molecular ions are formed with a significant amount of vibrational ex-

citation energy. It is a major problem to obtain N_2^+ in its $v=0$ level only. In an ion source, direct electron impact ionization of $N_2(X\ ^1\Sigma_g^+)$ produces some vibrational excitation in the $N_2^+(^2\Sigma_g^+)$ directly but even more by the (Meinel band) radiative cascading from the $A\ ^2\Pi_u$ excited state. The storage time of seconds possible in an ion storage ring effectively removes the $A\ ^2\Pi_u$ excited state. However, it is not possible to radiatively cool the vibrational population in the $^2\Sigma_g^+$ ground state. The homonuclear $^{14}N_2^+$ does not have the required electric dipole moment. Although isotopic substitution in the form of the $^{14}N^{15}N^+$ isotope results in a finite dipole moment, the associated radiative lifetime is too large for cooling in a reasonable amount of time. Nevertheless, Kella *et al.*[12] used $^{14}N^{15}N^+$ and found excited levels up to at least $v=3$ in an experiment to determine the final product state populations at 0 eV collision energy. These authors did not measure cross sections. We sought an alternative solution for $^{14}N_2^+$ by using a cooled hollow cathode ion source, which we have named JIMIS, similar to the one developed at SRI International.[32] It operates at relatively high pressures near 1 Torr to permit collisional deactivation of vibrationally excited levels. During the present experiments the pressures were reduced to about 0.3 Torr (measured just upstream of the source) in order to maximize the ion current yield. The ion source is small and cylindrical, with a radius of 6 mm. The 15 mm long copper cathode is water cooled to room temperature, and is separated 5 mm from the thin (0.05 mm) Mo exit foil, which has a 0.4 mm diam aperture on the beam axis. The copper anode, also 6 mm radius, is located behind (upstream from) the cathode. The discharge is struck with a cathode-anode voltage of about 900 V. The source is very stable with a series resistor of about 126 $k\Omega$, a discharge voltage of about 360 V, and a current of about 4.4 mA. The power dissipation was only 1.5 W in the source. The ion beam was about 40 nA. Significant cooling was evident from a comparison with results using the normal CRYRING hot filament discharge source MINIS, but excited states up to $v=3$ were still observed.

B. Time and position sensitive detector

A time and position sensitive detector forming a ''three-dimensional'' imaging detector (3D-ID) was used in this experiment. Three-dimensional refers to the combined measurement of the separation between the DR fragments (x, y coordinates) and their arrival-time interval (t). The explicit determination of the arrival time-difference between the two DR fragments makes it possible to really measure the kinetic energy of both fragments more accurately. Only in one case has 3D-imaging been reported before in ion storage ring experiments.[33,34] Fragments from a DR event in the electron cooler, unaffected by the bending magnets, progress in a straight line and strike the front of a set of three Microchannel plates (23 mm diam), ultimately producing scintillation on a phosphor screen (type P46, DEP Electronic Instruments, The Netherlands). The phosphor is imaged on to a high frame rate CCD (charge-coupled device) of size 1 mm^2 and 64×64 pixels (Dalsa Inc., Canada). The spatial resolution of the detector setup was ~0.3 mm. The complete detection system is operated in a gated mode to reduce unwanted signal in each CCD frame. This is achieved by reducing the voltage on the first MCP with a fast switch (250 V/μs) following the detection of light (and thus an event) from the phosphor by a fast PMT (Hamamatsu Photonics, Japan: Rise time typically 140 mV/ns).The same signal from the PMT constitutes the system trigger providing a reference for CFD (constant fraction discriminator) veto pulses, the ADC measuring gate, and the CCD frame grabber (BitFlow Inc., Canada).

Timing information is provided from 16 gold strips that have been evaporated on the surface of the last MCP. The strips are 0.8 mm wide with a spacing of 0.2 mm. The signals from the strips are amplified and fed into a 16 channel CFD (LeCroy model 3420). An ADC (LeCroy model 4300) then reports the length of the CFD outputs, the difference in which constitutes the arrival time interval between particles at the detector. The uncertainty in the timing measurement was assessed for a zero timing interval, and found to be in the region of 500 ps (i.e., $\Delta t_{\text{measured}}=\Delta t_{\text{absolute}}\pm250$ ps). The timing information is downloaded to a computer via a GPIB interface, and correlated with the camera frame. Operated in this mode, the maximum acquisition rate of the entire system is about 120 Hz, and limited, unfortunately, by the GPIB interface.

The 3D information provides the relative velocity of the fragments and hence their kinetic-energy release value. The quality of the position information is higher than that of the timing. Without timing information, the distribution of distances for events over a two-dimensional imaging detector is given by[3,12]

$$P(R)\approx\frac{1}{\Delta L}\int_{L_1}^{L_2}F\,\frac{R/R_{\max}}{R_{\max}\sqrt{1-(R/R_{\max})^2}}\,dL, \tag{1}$$

where $L_2-L_1=\Delta L$ is the cooler length, L_1 is the distance from the detector to the cooler, and $R_{\max}$ is the maximum projected distance on the detector for a given kinetic-energy release (ε). We used the timing information as a selection, effectively generating spectra from the events which have their dissociation angle perpendicular to the beam axis. This effectively increases the resolution of the detector. The selection is given by the parameter F

$$\text{where}\begin{cases}R<R_{\text{cut}}(L) & F=0\\ R>R_{\text{cut}}(L) & F=1\end{cases}$$

and where $R_{\text{cut}}(L)$ is determined from:

$$R_{\text{cut}}^2(L)=\frac{\varepsilon(m_1+m_2)L^2}{\mu E_0}-\tau_{\text{cut}}^2 v_0^2. \tag{2}$$

Here, R_{cut} is the distance on the detector for a given kinetic-energy ε (with ion beam energy E_0, velocity v_0, and for particle masses m_1, m_2, and reduced mass μ) and for a timing interval of τ_{cut} (in this case $\tau_{\text{cut}}=800$ ps) between fragments. That is, R_{cut} is the smallest distance separation that should be observed on the detector, after rejection of events with a timing interval greater than τ_{cut}. The finite

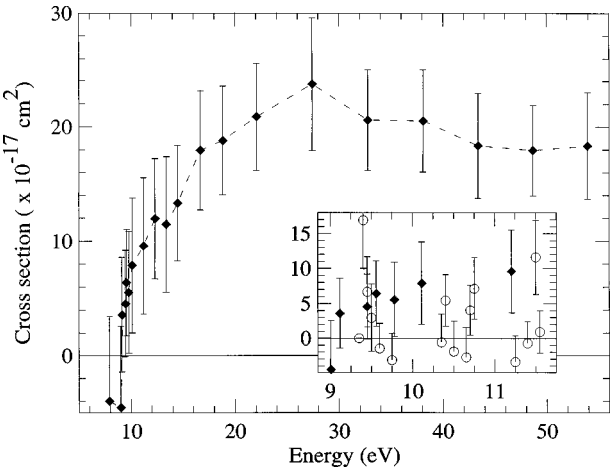

FIG. 2. Results of the dissociative excitation experiment. The inset shows a detailed comparison of the present data with those of Ref. 25 taken close to threshold (♦ present results, ○ from Ref. 25).

resolution in time has the effect of smearing the distributions over R_{cut}. Therefore, the model includes a calculation of the probability that fragments appearing with separation R will be either accepted ($\tau < \tau_{\mathrm{cut}}$) or rejected ($\tau > \tau_{\mathrm{cut}}$) due to the uncertainty in the timing. F is chosen to be

$$F = 1 - \left\{ \frac{\int_{\tau_{\mathrm{out}}}^{\infty} e^{-(\tau-\tau_R)^2/2\sigma^2} d\tau}{\int_{-\infty}^{\infty} e^{-\tau^2/2\sigma^2} d\tau} \right\}, \tag{3}$$

where τ_R is the time interval that corresponds to a separation R and for a given kinetic-energy release, and where σ represents the timing resolution [$\sigma = 210$ ps, FWHM (full width at half maximum) 500 ps]. The above procedure rejects events with small angles of dissociation (small with respect to the beam direction). The cutoff in angle depends on the magnitude of the kinetic energy. Hence the intensities of features in the spectra are not directly proportional to the branching ratios.

III. RESULTS

A. DE measurements

The cross sections for dissociative excitation of N_2^+ are shown in Fig. 2. These data were derived from MCS spectra of the N channel from the SBD. Corrections had to be made to the data to allow for the fact that the slow trapped-ion background B_t was time varying after switching energies. This is ascribed to the fact that the ionization cross section of the background gas is a function of the laboratory electron energy and that the trap depth changes with electron density. Thus, care had to be taken to obtain data soon after a jump in electron energy before the trapped ion population could change significantly. Without this precaution, ''false'' DE signals could be obtained well below the energetic threshold for the process.

The changes in the measured DE-rates were converted to the absolute cross sections shown in Fig. 2 by division by the relative velocity and correcting for the changes in electron density upon making the electron energy jumps. Already very close to the dissociation energy of the N_2^+ ground state of 8.724 eV some DE signal is observed. The DE cross section then increases very rapidly with excitation energy without showing particular structure. No information on the vibrational population can be obtained. The occurrence of dissociative excitation close to threshold is also found in H_2. In this process, formation of doubly excited neutral H_2 repulsive curves is invoked. These neutral states may auto-ionize during the dissociation to give $H + H^+ + e^-$. The HeH molecule does not have doubly excited neutral curves near the dissociation energy of its ionic ground state. As a consequence, no DE is observed at energies close to the binding energy of the ionic ground state.[5] The measured cross section for N_2^+ assumes a value of 2.2×10^{-16} cm^2 near 25 eV. It is of interest to note that the cross sections for production of N^+ fragments by electron impact on N_2^+ were measured by Van Zyl and Dunn.[35] Such cross sections are the sum of the DE cross section plus twice the cross section for dissociative ionization ($e^- + N_2^+ \rightarrow 2N^+ + 2e$). We return to this subject in the discussion. DE cross sections were measured also by Noren *et al.*[25] This single-pass experiment produced cross sections of similar magnitude to the data of Fig. 2. These measurements were primarily undertaken to probe the internal states of the ions, and the lack of precision makes it difficult to make a detailed comparison. One other feature that possibly deserves note, however, is that Noren *et al.* apparently observed some very sharp resonances in the DE cross section.[25] Unfortunately, our data were taken at energies that just miss probing for the reality of these resonances.

B. DR measurements

The procedure for the determination of the absolute DR rates requires information on the number of ions during the experiment. This information is extracted from the number of counts in the background channel of the SBD spectrum. We have applied a correction for the increase in background due to the DE process as well as for the increase due to ion trapping in the electron beam. The signal in the N_2-channel was corrected for the charge transfer contribution. This contribution was measured at three different collision energies. As expected, the same ratios were found between the N-atom and the 2N channel (charge transfer). Both processes scale proportionally to the residual gas pressure.

Absolute DR rates over a large collision energy range have been obtained by measuring in an independent experiment the absolute current in the ring (using a calibrated current transformer) in conjunction with the count rate in the background channel. Figure 3 shows the results from the two ion sources JIMIS and MINIS. The JIMIS data are shown as solid diamonds, those from MINIS are open circles. The spread in electron energy is about 10 meV. This spread dominates the resolution in the center of mass collision energy below 100 meV. Due to the threshold behavior ($\sigma \approx E^{-1}$ near $E = 0$ eV), an experiment at $E < 10$ meV is still useful. For example, the rate observed at a setting of $E = 0.001$ eV was already reduced by a factor of 2.7 with respect to the rate at cooling energy ($E = 0$ eV). Above 100

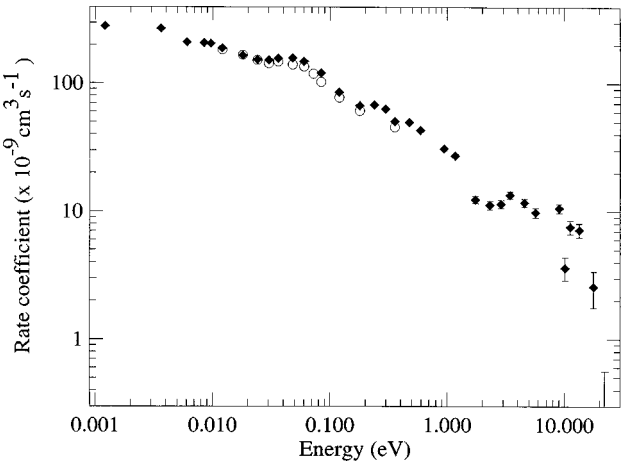

FIG. 3. Observed absolute DR rates for JIMIS (◆) and MINIS (○) between 2 meV and 20 eV. The rate of JIMIS is higher by 15% at $E=0.06$ eV.

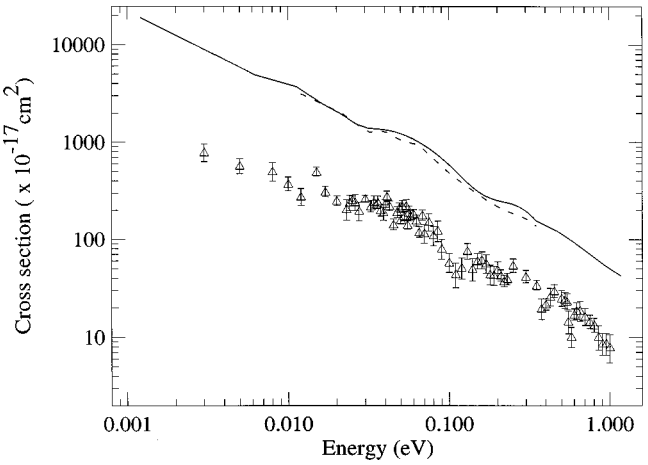

FIG. 4. Absolute DR cross sections as deduced from the absolute rates using a deconvolution procedure for the data below 100 meV and a simple division by the average collision velocity at elevated energies. JIMIS: —, MINIS: ----. Ref. 25:. Δ.

meV the energy resolution slowly decreases ($\approx E^{1/2}$) for kinematic reasons. To our surprise, the two ion sources give very similar results. Since, as will be described below, JIMIS is associated with a vibrationally colder molecular ion beam, we conclude that the rates cannot be strongly dependent on the vibrational quantum number. The ''colder'' source has a larger rate around 80 meV by about 15%, suggesting a rate that is higher for the $v=0$ level than for the $v=1$ level. Neither curve displays a lot of structure, the sharp minimum found at 8 eV has not been corroborated with more detailed experiments in the same energy region. At collision energies above 10 eV, negative rates were found, indicative of a small systematic error in correcting for charge transfer collisions between N_2^+ ions and residual gas. This error prevents the observation of rate coefficients below 1×10^{-9} cm^3 s^{-1}. The error bars in the rate coefficient in Fig. 3 include the subtraction procedure to correct for the charge transfer background; $\sigma(E)=[S(E)+2B(E)]^{1/2}$ with S the total signal, and, B the background.

Figure 4 shows the results of a deconvolution procedure to correct the rates for the energy spread in the electron beam to yield the absolute cross sections. The cross section curve (solid line) is shown for the JIMIS source (for which more data were taken) and can be described between 0.1 and 1 eV by $\sigma\approx E^{-1}$. For comparison, the cross-section data obtained by Noren *et al.*[25] have been included in Fig. 4, revealing that their data roughly give the correct trend between 20 meV and 1 eV. Their cross sections, however, are about five times lower at 0.07 eV. Both sets of data show similar undulations. We note that even out to 20 eV, the cross section does not have a maximum, as appears in other small diatomic species such as H_2[3,4,36,37] and HeH[5,6] and also in polyatomics such as H_3,[8] D_3,[38] H_3O, and CH_3.[10] For many of these systems a suitable repulsive potential among the ionic curves is known to be responsible for a maximum at high electron energy. Molecular nitrogen may not have such a state that is accessible in transitions from the N_2^+ equilibrium position. The fact that the higher mass of N_2 slows down the dissociation process and increases the importance of auto-ionization during dissociation may play a stronger role.

The cross section data have been converted to the often used electron temperature dependent rate coefficient as shown in Fig. 5. A comparison is made with earlier determinations using various techniques. The data are well fitted with the function $\alpha(T_e)=1.70\pm0.09\ \ 10^{-7}\ (T_e/300)^{-0.30\pm0.09}$ cm^3 s^{-1}. This result agrees very well with the calculations of Guberman,[39] who found $\alpha(T_e)=1.6\times10^{-7}(T_e/300)^{-0.37}$ cm^3 s^{-1}. We note that the ion kinetic and internal ''temperatures'' are, of course, the same for all electron temperatures. These internal temperatures cannot be quantified at this moment (see next section). The ion kinetic temperature is negligible. Despite the fact that we operated with a rather poor translational cooling of the ion beam, the relative ion spread velocity was still better than 10^{-3}. As a consequence, the centre of mass electron collision energy

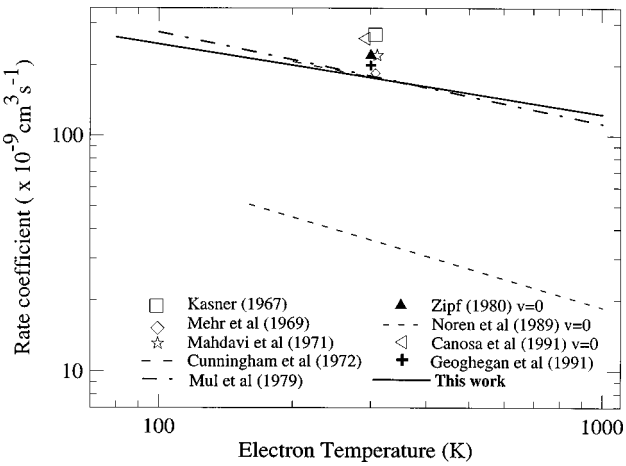

FIG. 5. Electron temperature-dependent rate coefficients as deduced from the present experiments (solid line) and the results from literature. Reference 19, ◇ Ref. 20, ☆ Ref. 21, ▲ Ref. 23, + Ref. 26, ◁ Ref. 27. The lines are: ------ Ref. 25, — This work, -- Ref. 22, —·— Ref. 52.

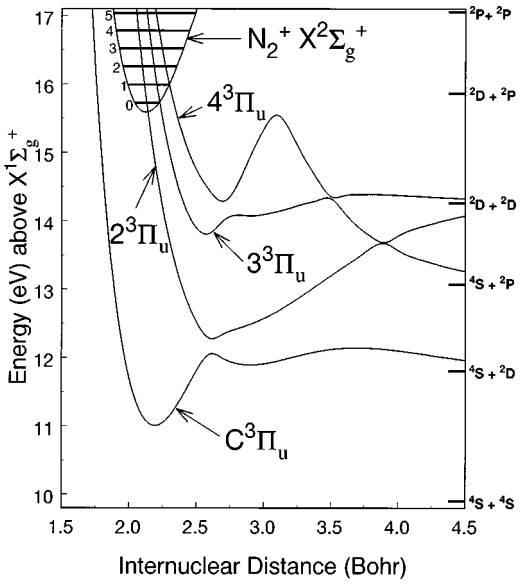

FIG. 6. Potential-energy diagram of molecular nitrogen and its ion. The ionic ground state is given with a selection of (doubly) excited repulsive neutral valence states. Note that none of the given repulsive curves correlate with ground state fragments, $N(^4S^0)+N(^4S^0)$. Also note the irregular shaped repulsive $^3\Pi_u$ curves, indicative for a large number of avoided crossings which can result in distribution of outgoing flux over the various dissociation limits.

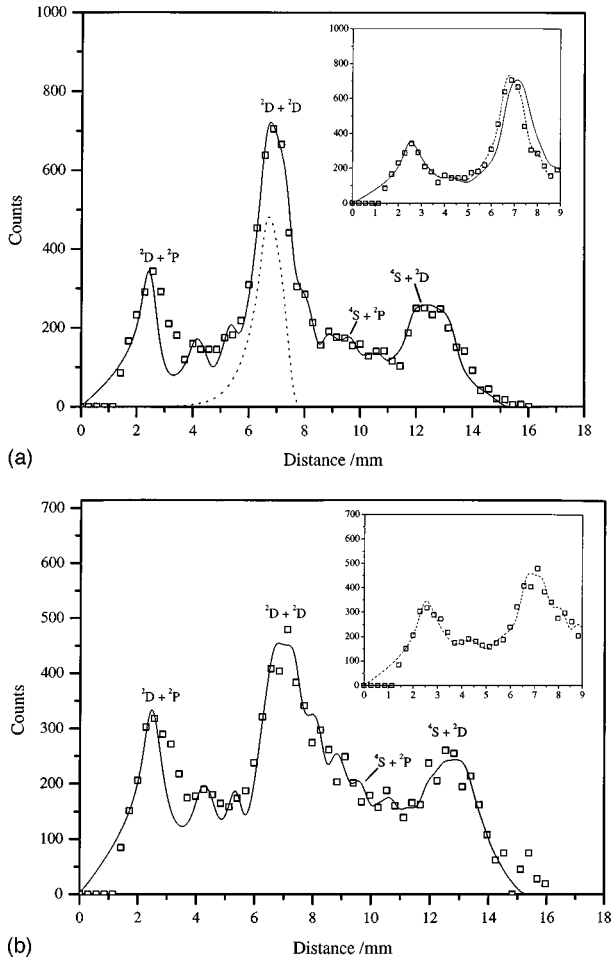

FIG. 7. 3D-ID spectra taken at 0 eV collision energy using JIMIS (a) and MINIS (b). The solid curve is a model spectrum. The intensity of each vibrational feature (determined by ion beam population, specific rate, and branching) has been optimized. The dashed line in (a) is the model spectrum of a single vibrational feature, $N_2^+(v=0)\rightarrow N(^2D)+N(^2D)$ at $T_{rot}=300$ K. The insets show spectra obtained using a rotational temperature $T_{rot}=1400$ K for the low-energy features and $T_{rot}=300$ K for the high-energy peak (dashed line). For comparison, the solid line is a spectrum with $T_{rot}=1400$ K for all features (solid line).

spread is still dominated by the temperature of the electron beam.

We note that surprisingly good agreement is found between all reported experiments on N_2^+, using different techniques and undoubtedly with a variation in vibrational composition. This can now be rationalized, since the DR rates from our two ion sources with markedly different vibrational populations were about the same.

C. Product state and vibrational populations

In order to understand the product state measurements using the three-dimensional imaging detector (3D-ID) as described in the experimental section, it is necessary to give more details on the molecular structure of N_2. The appropriate potential-energy curves have been calculated by Guberman[39] and are shown in Fig. 6. This figure shows that upon recombination of zero-energy electrons with N_2^+ ions a number of dissociation limits are accessible. These limits and the associated total kinetic energy of the fragments at 0 eV electron collision energy are

$$N_2^+(v^+=0)+e^-\rightarrow N(^4S)+N(^4S)+5.82\ \text{eV} \quad \text{(a)}$$

$$\rightarrow N(^4S)+N(^2D)+3.44\ \text{eV} \quad \text{(b)}$$

$$\rightarrow N(^4S)+N(^2P)+2.25\ \text{eV} \quad \text{(c)}$$

$$\rightarrow N(^2D)+N(^2D)+1.06\ \text{eV} \quad \text{(d)}$$

$$\rightarrow N(^2D)+N(^2P)$$

$$-0.13\ \text{eV}(\text{accessible for } v>0). \quad \text{(e)}$$

A few neutral repulsive states of $^3\Pi_u$ symmetry that connect the ionization region with the different dissociation limits are indicated. According to calculations by Guberman, the $2^3\Pi_u$ state plays an important role in the DR of N_2^+ $(v=0)$.[39] The clear presence of series of avoided crossings implies that it is not *a priori* obvious which dissociation limit will be chosen by nature.

The results from the 3D-ID from the two ion sources are shown in Fig. 7. Figure 7(a) shows data from the cooler source JIMIS, and Fig. 7(b) is from the ''hot'' source MINIS, both taken at the cooling energy, thus $E=0$. Each spectrum gives the distribution of distances between the two fragments. The spectra show distance distributions of events with a difference in arrival time smaller than 800 ps, for which the fragments dissociated perpendicularly to the beam axis. In this case, the fragment distance is proportional to the square root of the kinetic energy of the fragments. The dominant peak in the middle of Fig. 7(a) reflects the formation of

two $N(^2D)$ atoms [Channel (d)] starting from N_2^+ $(v=0)$ and leaving 1.1 eV for the total kinetic energy released. The width of this peak is dominated by the uncertainty of the position of the DR reaction in the electron cooler. This uncertainty ($\Delta L=0.85$ m, $L=6.3$ m) gives a 15% spread in the observed distances ''d''. The highest energy channel, producing two ground state $N(^4S)$-atoms, is not observed. This spectrum qualitatively agrees with that of Kella *et al.*[12] Superimposed on the data is a model spectrum that is built up from contributions to different dissociation limits, and which includes electron capture by vibrationally excited N_2^+ $(v=1-3)$. Inclusion of $v=4$ does not improve the fit. In the model, populations of the different vibrational states and the branching were free parameters. A rotational temperature was assumed in accord with the properties of the source, for JIMIS $T=300$ K, for MINIS with a heated filament in the source, $T=600$ K. In this temperature range, only the structures at very small kinetic energy (small d values) are affected. A *quantitative* fitting of the spectrum to yield branching ratios and apparent vibration populations in the N_2^+ ion beam requires information on the N_2^+ beam size. It was found that the size of the beam is comparable to that of the detector (diameter 23 mm) at 6.3 m behind the cooler. As a consequence, high kinetic-energy events have a smaller detection probability. From an analysis of all events, the ion beam profile has been obtained and an energy dependent detection efficiency has been determined. The three major peaks contain contributions from vibrationally excited N_2^+ ions. The shoulder near $d=7.5$ mm is the $v=1$ contribution to $N(^2D)+N(^2D)$. Because of the large energy difference between the different N+N dissociation limits, we can observe not only the branching of each vibrational state over the different dissociation limits but also obtain an estimate of the vibrational population in the ion beam. The structure at small distances d is ascribed to N_2^+ $(v=1)$ dissociating to $N(^2D)+N(^2P)$. The energy of the N_2^+ $(v=0)$ level is insufficient to arrive at this limit for zero-energy electrons. For very small distances between the fragments we cannot reproduce the shape of the observed spectrum using the expected rotational temperature, which fits the higher energy peaks. The oscillations in the model spectrum reflect the contributions from $v=1$,2, and 3. The spectrum agrees at low energy with that of Ref. 12. If we use the temperature used in Ref. 12 of 1400 K we arrive at model spectra as given in the insets of Figs. 7(a) and 7(b). The peak at small energy shows a better fit but the shoulder at the dominant peak $[N(^2D)+N(^2D)]$ attributed to the $v=1$ disappears. The peaks also shift due to the increased rotational temperature and the agreement of the model spectrum and the observed spectrum decreases. This is more clearly the case in Fig. 7(a). We conclude that most features can be described by a lower rotational temperature. The cause of the high temperature of the first peak is not due to a DR-rate which strongly increases with the rotational quantum number. Hence, we conclude that the probability of dissociation to the $N(^2P)+N(^2D)$ limit increases with rotational quantum number. Note that a change of 0.1 eV in rotational energy is a significant change in the asymptotic kinetic energy. Also note, that the $v=2$ and $v=3$ features at $d=4$ and $d=5$ mm are also better reproduced, which may imply that a heterogeneous J-dependent coupling mechanism is responsible for the branching to the $N(^2P)+N(^2D)$ limit.

TABLE I. Branching behavior of $N_2^+(v=0)$ level and the contribution of each vibrational level to the spectrum. The latter are the products of ion beam population and vibration specific DR-rate. Results are given for both ion sources.

Ion source	Product channel	Branching ratios $(v=0)$	v	Vibrational distribution (population x rate)
JIMIS	$^4S+^2D$	$37\pm8\%$	0	46%
	$^4S+^2P$	$11\pm6\%$	1	27%
	$^2D+^2D$	$52\pm4\%$	2	10%
			3	16%
MINIS	$^4S+^2D$	34%	0	30%
	$^4S+^2P$	19%	1	31%
	$^2D+^2D$	47%	2	19%
			3	18%

The branching over the different dissociation limits as well as the intensities of the different vibrational levels are collected in Table I. We point out that the outcome of the simulations are products of the population and a state-specific DR rate. The results are: The lowest energy dissociation limit, Channel (a), is not found, Channel (d) with two $N(^2D)$ atoms is the strongest channel. Furthermore, the ion source JIMIS produces significantly cooler ions (vibrationally) than the MINIS source. The ratio of $v=0$ to $v=1$ signal levels from JIMIS is greater by 80%. As has been described, this difference affects the observed DR rates by less than 10%. Hence, with moderate reservation, we can conclude that the relative signal strengths of the $v=0$ and $v=1$ levels reflect the populations in the beam. Table I gives the contributions of the different vibrational levels to the total spectrum. Note that the numbers for the JIMIS source (46%, 27%, 10%, 16%) are not monotonically decreasing. Since these numbers represent a product of ion beam population and state specific rate, this result may indicate a drop in the specific DR-rate for the $v=2$ level or an increase in the specific rate for the $v=3$ level, maybe due to an advantageous curve crossing with a higher lying repulsive curve. No evidence has been found for contributions from vibrational levels greater than $v=3$. The same cutoff was found in the experiment at the ion storage ring ASTRID by Kella *et al.*,[12] who noted that this cutoff ''$\cdots$may be explained by the proximity of the $A\ ^2\Pi_u$ state, whose $v=0$ level is just above $v=4$ of the $X\ ^2\Sigma_g^+$ ground state.'' Thus levels $v=5$ and higher can radiate to the A state $v=0$, which in turn radiates to lower levels of the ground state in about 10 μs.[40] It is not entirely clear that the cutoff is really at $v=3$, at least for the MINIS source and in the Århus case (which was even hotter, with poorer resolution). But in the JIMIS analysis, the population of $v=3$ was small enough that inclusion of $v=4$ would have been meaningless. In any case, we were primarily interested in the fate of $v=0$, which is important in atmospheric applications, and whose contribution and

branching is more clearly separable from the higher levels.

The rate coefficients do not change much with vibrational quantum number, in contrast to the situation in H_2 where evidence has been found that the cross section of the different vibrational levels can differ by two orders of magnitude or more.[4] In N_2^+ this behavior may be due to the greater abundance of curve crossings between the various $^3\Pi_u$ curves with the N_2^+ curve. The DR branching behavior of N_2^+ $v=0$ ions reported from the ion storage ring ASTRID agrees only qualitatively with our observations. Channel (c) is least favored, but we find branching to channels (b), (c), and (d) in the ratios b:c:d=$(37\pm8)\%$:$(11\pm6)\%$:$(52\pm4)\%$, while Kella *et al.*[12] reported using a two-dimensional imaging technique $(46\pm6)\%$:$(8\pm6)\%$:$(46\pm6)\%$. As mentioned before, for a satisfactorily fit they had to use an overall rotational temperature of 0.12 eV (1400 K).

For the $v=0$ state the main DR route has been believed to be via the $2\,^3\Pi_u$ state (also known as the $C'\,^3\Pi_u$ state). Guberman[39] has calculated that the direct coupling to $3\,^3\Pi_u$ at the outer turning point of $v=0$ is 60 times *weaker* than that of $2\,^3\Pi_u$, which crosses at the maximum in the vibrational wave function. The only efficient route to the channel (b) limit is by diabatically passing the avoided crossing of the $2\,^3\Pi_u$ state with the $C'\,^3\Pi_u$ state. Starting out on the $2\,^3\Pi_u$ state and adiabatically taking the avoided crossing with the $C\,^3\Pi_u$ state, the higher lying dissociation limits, (c) and (d) may be reached. The limit (c) is reached by adiabatic behavior at the crossing near 2.1 Å, and the limit (d) by diabatic behavior at this crossing. Theoretical calculations exist for these two avoided crossing situations. Guberman predicted a predominantly diabatic behavior at both these crossings near 1.4 and 2.1 Å. Hence, he predicted the lower (b) limit $[N(^4S)+N(^2D)]$ to dominate. The yield in this channel was calculated to be 88% in a Landau–Zener calculation that considered only the $2\,^3\Pi_u$ state, and 70% in a later calculation that included other $^3\Pi_u$ states.[39,41] The diabatic character at the crossing at 2.1 Å, resulted in fractional yields for the limits (c) and (d) of 0 and 12%,[39] and 3%, and 27%, respectively.[41] Our results are clearly not in agreement with these predictions.

It is worth mentioning that in photodissociation studies the $2\,^3\Pi_u$ state has also been invoked in predissociation of $n=3$ and $n=4$ singlet Rydberg and valence excited states 2 eV below the ionization energy. In these studies, only the lower three (a)–(c) dissociation limits were energetically accessible.[42–46] Predissociation of these lower Rydberg levels never reaches the $N(^4S)+N(^4S)$ limit, an observation consistent with the present results for DR. The predissociation studies reveal a complex pattern of branching to the $N(^4S)+N(^2D)$ and $N(^4S)+N(^2P)$. The branching here can change even as function of rotational levels within one vibrational level.[43] Hence, no clear conclusion can be drawn regarding whether the avoided crossing between the C and $2\,^3\Pi_u$ states is dominantly diabatic as suggested by theory. If the behavior at this crossing indeed is dominantly diabatic, then the premise, that the electron capture process involves only the $2\,^3\Pi_u$ state, may be incorrect.

The $^2D+^2P$ limit is energetically inaccessible from $v=0$, but the $v=1-3$ levels can give all five, (a)–(e), limits. The $3\,^3\Pi_u$ and $4\,^3\Pi_u$ states may both play a role for the $v=2$ to 3 levels. The fact that the branching of the $v=1-3$ states seems to be roughly the same within the considerable error bars, suggests that electron capture for those levels may be dominated by one electronic state which correlates with different products.

IV. DISCUSSION

Dissociative recombination typically takes place via two mechanisms. The first is simply by direct excitation to a repulsive state of the molecular ion. The second is by resonant capture in Feschbach resonances, which are Rydberg states converging to one of the ionic states. These resonances can stabilize through dissociation, thus ending in DR. Provided that these resonances are sufficiently high in energy, they can autoionize to ionic states in their dissociation continuum. The latter process is called (resonant) dissociative excitation (DE) and competes with the DR process. This competition has been observed in HD^+, HeH^+, and D_3^+ (Refs. 4, 5, and 38, respectively). At elevated collision energies, the shape of the DR resonance is very similar to that of the DE process. In N_2^+, we observe no ''high-energy'' resonance features in either the DR or the DE cross sections. One may speculate that resonant DE is not operative. Yet, the threshold for DE seen in Fig. 2 is so close to the binding energy of the N_2^+ ground state, that one must conclude that there are ''very flat'' repulsive ionic curves or neutral Feschbach resonances in the region of the bound ionic state. In 1979 the cross section for N^+ (and N_2^{2+}) production was measured using electron impact and crossed beams.[35] The cross section is the sum of dissociative excitation, ionization and dissociative ionization (DI): $\sigma=\sigma_{DE}+\sigma_I+2\sigma_{DI}$. In that work the measurements were carried out to 500 eV, and the results were fitted to $\sigma_m=(923/E)\log_{10}E-(1411/E)$ with E in eV and σ in units of πa_0^2. In the present experiments we only measure σ_{DE}. After fitting our DE data (>20 eV) to $A/E\ln E+B$, we can obtain the sum of $\sigma_I+2\sigma_{DI}$ by subtracting the data of Fig. 2 from the older set of data of Ref. 31. If we assume that the double ionization cross section (σ_I; N_2^{2+} formation) is much smaller than σ_{DI}, we can obtain a reasonable estimate of this latter cross section, σ_{DI}, $N_2^+ + e^- \rightarrow N^+ + N^+ + 2e^-$. We note that the asymmetric dissociative ionization process, $N_2^+ + e^- \rightarrow N^{2+} + N + 2e^-$, which would contribute to our DE signal has a cross section smaller than 10^{-18} cm^2 below 100 eV.[47] Figure 8 shows the results of this procedure, together with calculations by Kim of the total ionization cross section based on the binary-encounter-Bethe (BEB) model,[48] developed by Kim and Rudd.[49] This model uses the ground-state wave function of the target molecule. The two different theoretical curves are based on different choices for the N_2^+ ground-state wave function. Considering the sizable uncertainties, the agreement is very good. It should be pointed out that there is a paucity of data for DI of molecular ions. The only other

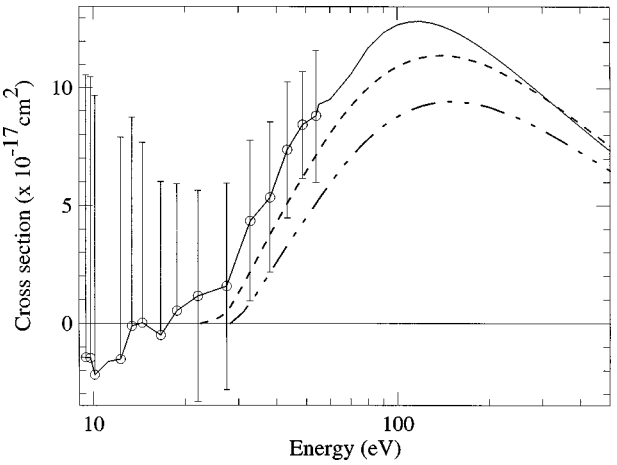

FIG. 8. Dissociative ionization cross-section data as derived from the DE cross sections (Fig. 2) and literature data (Ref. 35). The solid curve and points are experimental data. The other two lines are theoretical determination of the total ionization cross section of N_2^+ using different ground-state wave functions of the target N_2^+ molecule (see text for details).

measurements[50] are for H_2^+ and a recent measurement[51] for CD^+. The latter was determined with a method similar to the present work.

We now discuss the DR rates. Previous measurements have been reviewed by Fox.[13] We found a rate coefficient of $1.75\pm0.09\times10^{-7}(T_e/300)^{-0.30\pm0.02}$ cm^3 s^{-1}. This result compares quite favorably with the 300 K rate coefficients of 2.2×10^{-7} cm^3 s^{-1} found by Zipf[23] and $1.6\times10^{-7}(T_e/300)^{-0.37}$ cm^3 s^{-1} calculated by Guberman.[39] Mehr and Biondi,[20] from a microwave afterglow measurement, found a similar $T_e^{-0.39}$ dependence with a 300 K rate coefficient of 1.8×10^{-7} cm^3 s^{-1}. Mul and McGowan[52] measured 3.7×10^{-7} cm^3 s^{-1} at 300 K, but it was later corrected downward to 1.8×10^{-7} cm^3 s^{-1}.[25] From shock tube measurements, Cunningham and Hobson[22] reported an extrapolated rate coefficient of $1.78\times10^{-7}(T_e/300)^{-0.37}$ cm^3 s^{-1}, and Noren *et al.*[25] reported the previously mentioned 300 K low value of 3.6×10^{-8} cm^3 s^{-1}. Thus, most 300 K rates are very similar to those reported here, but we found a somewhat smaller temperature dependence of $T_e^{-0.30}$.

One of the important questions asked about the DR products from $v=0$ is what fraction ends up in channel (b), which is important in allowing the escape of ^{14}N from the Martian atmosphere following the DR of $^{14}N^{15}N^+$, thus affecting the isotopic balance, as mentioned in the Introduction. The situation was reviewed in detail by Fox.[14] Our yield of about 37% is lower than the data by Kella *et al.*[12] 46%. The experiments give definitely less than that of Guberman, who found 88% and later 70% by including other $^3\Pi_u$ states,[39,41] and more in line with the 24% of Fox and Dalgarnov[53] in an earlier model, which assumed that the channels were produced in a statistical distribution (see Fox, Ref. 16, p. 3306). Queffelec *et al.*[54] deduced a branching smaller than 15%.

One other aspect of our measurements should be mentioned. We have concluded that the DR rates do not depend much on the vibrational state. At least we saw no evidence of drastic changes. Similar behavior was seen in the shock tube studies of Cunningham and Hobson,[22] and by Torr and Orsini,[55] who reexamined data taken by the Atmospheric Explorer. Probably the most significant study was that of Zipf.[23] In a laser fluorescence study, he measured the disappearance rates of $v=0-2$ in the afterglow of a plasma, and obtained 300 K rate coefficients of (2.1, 2.4, and 2.7)$\times10^{-7}$ cm^3 s^{-1}. The findings of Zipf and the present results dispute earlier speculations of Orsini *et al.*[56] that DR in N_2^+ increases strongly with $v>0$.

The complexity of N_2^+ defies simple intuitive arguments. The relative insensitivity of the DR-rate to the vibrational level in combination with the branching behavior is very interesting. The $2\,^3\Pi_u$ repulsive state cannot dominate the DR process. Then the rate would change dramatically from vibrational level to vibrational level, because of rapidly varying overlap integrals. Hence, other repulsive states do play a role in the electron capture process. So, these results indicate the interplay of various repulsive states. These states are also strongly coupled at larger internuclear separations, which affects the branching behavior. A more detailed theoretical study is in order for an adequately detailed understanding to be reached.

In conclusion, the present experiments have provided absolute rate and cross sections for dissociative recombination and dissociative excitation of N_2^+, with an at least partially known vibrational population in the N_2^+ ion beam. The branching of the different vibrational levels over the accessible dissociation limits has been determined semiquantitatively. The DR results of the present ion-storage-ring fast-beam experiment agrees with many of the earlier afterglow techniques. In the future, difficult but necessary improvements pertain to better control of the ion beam population, with ideally an N_2^+ $(v=0)$ beam only, and further improvements in the resolving power of the imaging detector in order to improve the information concerning the dissociation products.

ACKNOWLEDGMENTS

This work was supported by the Göran Gustafsson Foundation for Research in Natural Sciences and Medicine, the Swedish National Science Research Council and the Wenner-Gren Foundation. All of us are grateful to the staff of the Manne Siegbahn Laboratory for the high level of operation of the CRYRING International facility. One of us (G.H.D.) is grateful to the Swedish Royal Academy of Sciences and to the office of Fusion Energy, U.S. Department of Energy for support. This work is part of the research program of the Stichting voor Fundamenteel Onderzoek der Materie (FOM) and was made possible by financial support from the Nederlandse Organisatie voor Wetenschappelijk Onderzoek (NWO). We acknowledge discussions with S. L. Guberman, D. Zajfman, W. Walter, and P. C. Cosby on various aspects of the experiment. J. B. A. Mitchell is acknowledged for valuable discussions and sharing of original results. S. L. Guberman is thanked with providing us with Fig. 6.

[1] See *Dissociative Recombination: Theory, Experiment, and Applications III*, edited by D. Zajfman, J. B. A. Mitchell, D. Schwalm, and B. R. Rowe (World Scientific, Singapore, 1996).
[2] M. Larsson, Annu. Rev. Chem. Phys. **48**, 145 (1997).
[3] D. Zajfman, Z. Amitay, C. Broude, P. Forck, B. Seidel, M. Grieser, D. Hobs, D. Schwalm, and A. Wolf, Phys. Rev. Lett. **75**, 814 (1995).
[4] W. J. van der Zande, J. Semaniak, V. Zengin, G. Sundström, S. Rosén, C. Strömholm, S. Datz, H. Danared, and M. Larsson, Phys. Rev. A **54**, 5010 (1996); L. H. Andersen, P. J. Johnson, D. Kella, H. B. Pedersen, and L. Vejby-Christensen, *ibid.* **55**, 2799 (1997).
[5] C. Strömholm, J. Semaniak, S. Rosen, H. Danared, S. Datz, W. J. van der Zande, and M. Larsson, Phys. Rev. A **54**, 3086 (1996).
[6] J. Semaniak, S. Rosén, G. Sundström, S. Datz, H. Danared, M. af Ugglas, M. Larsson, W. J. van der Zande, Z. Amitay, D. Zajfman, U. Hechtfischer, M. Grieser, M. Repnow, M. Schmidt, D. Schwalm, and A. Wolf, Phys. Rev. A **54**, R4617 (1996).
[7] Z. Amitay, D. Zaijfman, P. Forck, U. Hechtfischer, B. Seidel, M. Grieser, D. Habs, R. Repnow, D. Schwalm, and A. Wolf, Phys. Rev. A **54**, 4032 (1996).
[8] S. Datz, G. Sundström, Ch. Biederman, L. Broström, H. Danared, S. Mannervik, J. R. Mowat, and M. Larson, Phys. Rev. Lett. **74**, 896 (1995).
[9] S. Datz, M. Larsson, C. Strömholm, G. Sundström, V. Zengin, H. Danared, A. Källberg, and M. af Ugglas, Phys. Rev. A **A52**, 2901 (1995).
[10] L. H. Andersen, O. Heber, D. Kella, H. P. Pedersen, L. Vejby-Christensen, and D. Zajfman, Phys. Rev. Lett. **77**, 4891 (1996); L. Vejby-Christensen, L. H. Andersen, O. Heber, H. B. Pedersen, H. T. Schmidt, and D. Zajfman, Astrophys. J. **483**, 531 (1997).
[11] J. Semaniak, Å. Larsson, A. Le Padellec, C. Strömholm, M. Larsson, S. Rosén, R. Peverall, H. Danared. N. Djuric, G. H. Dunn, and S. Datz, Astroph. J. (submitted).
[12] D. Kella, P. J. Johnson, H. B. Pedersen, L. Vejby-Christensen, and L. H. Andersen, Phys. Rev. Lett. **77**, 2432 (1996).
[13] J. L. Fox, in *Dissociative Recombination: Theory, Experiment, and Applications*, edited by B. R. Rowe, J. B. A. Mitchell, and A. Canosa (Plenum New York, 1992), p. 219.
[14] J. L. Fox, Planet. Space Sci. **40**, 1663 (1992).
[15] M. K. Wallis, Planet. Space Sci. **26**, 949 (1978).
[16] J. L. Fox, J. Geophys. Res. **98**, 3287 (1993).
[17] A. O. Nier and M. B. McElroy, J. Geophys. Res. **82**, 4341 (1977).
[18] M. A. Biondi and S. C. Brown, Phys. Rev. **76**, 1697 (1949).
[19] W. H. Kasner, Phys. Rev. **164**, 194 (1967).
[20] F. J. Mehr and M. A. Biondi, Phys. Rev. **181**, 264 (1969).
[21] M. R Mahdavi, J. B. Hasted, and M. M. Nakshbandi, J. Phys. B **4**, 1726 (1971).
[22] A. J. Cunningham and R. M. Hobson, J. Phys. B **B5**, 2328 (1972).
[23] E. C. Zipf, Geophys. Res. Lett. **7**, 645 (1980).
[24] R. Johnsen, Int. J. Mass Spectrom. Ion Processes **81**, 67 (1987).
[25] C. Noren, F. B. Yousif, and J. B. A. Mitchell, J. Chem. Soc. Faraday Trans. **85**, 1697 (1989).
[26] M. Geoghegan, N. G. Adams, and D. Smith, J. Phys. B **24**, 2589 (1991).
[27] A. Canosa, J. C. Gomet, B. R. Rowe, and J. L. Queffelec, J. Chem. Phys. **94**, 7159 (1991).
[28] M. Larsson, Int. J. Mass Spectrom. Ion Processes **149/150**, 403 (1995).
[29] C. Strömholm, H. Danared, A. Larson, M. Larsson, C. Marian, S. Rosén, B. Schimmelpfennig, I. F. Schneider, J. Semaniak, A. Suzor-Weiner, U. Wahlgren, and W. J. van der Zande, J. Phys. B (in press).
[30] H. Gao, Low energy electron-ion recombination at CRYRING, PhD thesis, Stockholm University, 1996.
[31] J. R. Mowat, J. Danared, G. Sundström, M. Carlson, L. H. Andersen, L. Vejby-Christensen, M. af Ugglas, and M. Larsson, Phys. Rev. Lett. **74**, 50 (1995).
[32] U. Müller and P. C. Cosby, J. Chem. Phys. **105**, 3532 (1996).
[33] D. Zajfman, Z. Amitay, M. Lange, U. Hechtfischer, L. Knoll, D. Schwalm, R. Wester, A. Wolf, and X. Urbain, Phys. Rev. Lett. **79**, 1829 (1997).
[34] Z. Amitay and D. Zajfman, Rev. Sci. Instrum. **68**, 1387 (1997).
[35] B. Van Zyl and G. H. Dunn, Phys. Rev. **163**, 43 (1967).
[36] C. Strömholm, I. F. Schneider, G. Sundström, L. Carata, H. Danared, S. Datz, O. Dulieu, A. Källberg, M. af Ugglas, X. Urbain, V. Zengin, A. Suzor-Weiner, and M. Larsson, Phys. Rev. A **A52**, R4320 (1995).
[37] I. F. Schneider, C. Strömholm, L. Carata, X. Urbain, M. Larsson, and A. Suzor-Weiner, J. Phys. **B30**, 2687 (1997).
[38] A. Le Padellec, M. Larsson, H. Danared, Å. Larsson, J. R. Peterson, S. Rosén, J. Semaniak, and C. Strömholm, Physica Scripta (in press).
[39] S. L. Guberman, Geophys. Res. Lett. **18**, 1051 (1991); S. L. Guberman, *Dissociative Recombination: Theory, Experiment, and Applications*, edited by B. Rowe, J. B. A. Mitchell, and A. Canosa (Plenum New York, 1992), p. 47; S. L. Guberman, *Dissociative Recombination: Theory, Experiment, and Applications*, edited by J. B. A. Mitchell, and S. L. Guberman (World Scientific, Singapore, 1989), p. 45.
[40] J. R. Peterson and J. T. Moseley, J. Chem. Phys. **58**, 172 (1973).
[41] S. L. Guberman (personal communication).
[42] H. Helm and P. C. Cosby, J. Chem. Phys. **90**, 4208 (1988).
[43] C. W. Walter, P. C. Cosby, and H. Helm, J. Chem. Phys. **99**, 553 (1993).
[44] C. W. Walter, P. C. Cosby, and H. Helm, Phys. Rev. A **50**, 2930 (1994).
[45] B. Buijsse, E. R. Wouters, and W. J. van der Zande, Phys. Rev. Lett. **77**, 243 (1996).
[46] B. Buijsse and W. J. van der Zande, J. Chem. Phys. (in press).
[47] A. Siari, D. S. Belic, P. Defrance, *XXICPEAC*, edited by F. Aumayr, G. Betz, and H. Winter (Vienna, Austria, 1997).
[48] Y. K. Kim (private communication).
[49] Y. K. Kim and E. Rudd, Phys. Rev. A **50**, 3954 (1994).
[50] B. Peart and K. T. Dolder, J. Phys. B **6**, 2409 (1973); **5**, 1554 (1972).
[51] N. Djuric, Y.-S. Chung, B. Wallbank, and G. H. Dunn, Phys. Rev. A. (submitted).
[52] P. M. Mul and J. Wm. McGowan, J. Phys. B **B12**, 1591 (1979).
[53] J. L. Fox and A. Dalgarno, J. Geophys. Res. **88**, 9027 (1983).
[54] J. L. Queffelec, B. R. Rowe, M. Morlais, J. C. Gomet, and V. Valée, Planet. Space Sci. **33**, 263 (1982).
[55] D. G. Torr and N. Orsini, Geophys. Res. Lett. **5**, 657 (1978).
[56] N. Orsini, D. G Torr, H. C Brinton, L. H Brace, W. B Hanson, J. H Hoffman, and A. O Nier, Geophys. Res. Lett. **4**, 43 (1977).